COLLISIONS AND FRACTURES: A PREDICTIVE THEORY

Francesco Freddi[1], **Michel Frémond**[2]

[1]Laboratorio Lagrange, Dept. of Civil-Environmental Engineering,
University of Parma, Parma, Italy
[2]Laboratorio Lagrange, Dept. of Civil Engineering,
Tor Vergata University, Rome, Italy
francesco.freddi@unipr.it (Francesco Freddi)

Abstract

We investigate collisions of solids which can fracture. Equations of motion and constitutive laws provide a predictive theory. Assuming the collisions instantaneous, the equations of motion in a damaging collision are derived from the principle of virtual work introducing new interior forces which describe the very large stresses and the very large contact forces resulting from the cinematic incompatibilities. They are interior volume percussion stresses and interior surface percussions both on the unknowns fractures and on the colliding surfaces. In order to approximate these equations, we assume solids are damageable. In this point of view, we may assume the velocity is continuous with respect to space but its strain rate is very large in a thin region where the material is completely damaged, so approximating a fracture. When the velocity before collision is very large, the damaged zone may be large accounting for parts of the solid completely transformed into powder. The constitutive laws result from dissipative functions satisfying the second law and able to model the fracturation phenomenon at the macroscopic engineering level. Representative numerical examples confirm that the model accounts for the fracturation and fragmentation qualitative properties. In particular, the model is able to reproduce real experimental tests.

Keywords: collision, principle of virtual work, fracture, damage.

Presenting Author's Biography

Francesco Freddi. He graduated in Civil Engineering at the University of Parma in 2000 and he received a Ph.D in Structural Mechanics at the University of Bologna in 2004. He had been Post-Doctoral Associate at the Laboratoires des Ponts et Chaussées in 2004 and 2005. He is member of the Laboratoire Lagrange since 2005. In 2006 he became Research Associate at the Department of Civil-Environmental Engineering at the University of Parma. His research interests lie in the area of computational and solid mechanics. Specifically, his research focuses on cohesive fracture mechanics, damage of glued materials, collision and fracture, FRP-concrete debonding, singular problem of elasticity, sulphation of porous stones, fracture of glass and related numerical methods.

ISBN 978-3-901608-32-2

1 Introduction

Collisions and fractures of solids are important engineering issues, for instance, fragmentation of solids by blasting, by collisions,... [1], [2].

The present work deals with collisions of deformable and damageable solids. In particular, we investigate the appearance of fractures due to collision. Collisions are phenomenons which occur in a very short period of time, they involve large impulsive forces in the bodies. We limit the investigation of this problem at the engineering macroscopic level and derive a model by discontinuous mechanics theory. We suppose that collision events are very short if compared with the duration of the other phenomena. Thus, we assume the collisions are instantaneous according to [3] and [4]. A collision is characterized by a time discontinuity of the velocity field: there is the velocity before collision $\mathbf{u}^-(\mathbf{x})$ and the velocity after collision $\mathbf{u}^+(\mathbf{x})$. A fracture is characterized by a spatial discontinuity of the velocity after collision $\mathbf{u}^+(\mathbf{x})$.

The predictive theory is based on the principle of virtual work giving the equations of motion and constitutive laws relating the internal forces to pertinent quantities describing the evolution. The equations of motion introduce interior percussion stresses, and percussions which result from the kinematic incompatibilities. They are interior volume percussion stresses and interior surface percussions both on the unknowns fractures and on the colliding surfaces. The constitutive laws are derived with dissipative potentials which fulfill the second law of thermodynamics. This collision theory applies to collision of either rigid or deformable solids [4] as well as of a solid colliding with an incompressible fluid [5].

In order to solve numerically the resulting set of partial differential equations (reference is made to [6] and [4] for details), we assume solids are damageable and that a damage quantity $\beta(\mathbf{x})$ with value 1 when the material is undamaged and value 0 when completely damaged. We consider that the damage quantity evolves rapidly in the collision: thus we assume it is discontinuous with respect to time at collision time : $\beta^-(x)$ before collision and $\beta^+(\mathbf{x})$ after. In this point of view, we may assume the velocity $\mathbf{u}^+(\mathbf{x})$ is continuous with respect to space but its strain rate is very large in a layer where the damage quantity $\beta^+(\mathbf{x})$ is almost zero, i.e., a fracture is approximated by a thin damaged zone where $\beta^+(\mathbf{x}) \simeq 0$, (this damage is 1 where the material is not fractured). When the velocity before collision is very large, the damaged zone may be large accounting for parts of the solid completely transformed into powder.

The variational formulation of the equations of motion is discretized by the classical finite element technique. Moreover, kinematic constraints on the velocity field $\mathbf{u}(\mathbf{x})$ are introduced in order to avoid overlapping phenomena along the contact surface and in the volume damaged zones. Finally, the discrete solution is obtained as a minimization of a non convex problem, reached through a specific method that couples descent technique and the Uzawa method. This scheme permits to account for the duality variables introduced by the constraints, for instance the impenetrability condition.

Several numerical simulations are proposed. Their aim is to demonstrate the capabilities of the predictive theory to describe qualitatively different failure modes occurring at collision time.

2 The Principle of virtual work

It is usual to derive the equation of motion through the principle of virtual power [3]. This principle can be used when all the quantities have densities with respect to the Lebesgue measure. When they have densities with respect to the atomic measure, as in the present situation, the principle of virtual power is advantageously replaced by the principle of virtual work. The principle of virtual work we use here, is not to be confused with the principle of virtual power where the velocities are understood as small displacements. This relation is often also called in a misleading way, the principle of virtual work.

For the sake of simplicity, let us consider a deformable solid Ω colliding a rigid fixed obstacle on $\partial\Omega_1$. Due to the kinematic incompatibilities very large interior forces appear within the solid, along the contact surface and on the unknown fracture surfaces. We consider the duration of the collision is very short, i.e., the time for the velocities to adapt to the presence of the obstacle is very short. Thus we assume the collision as instantaneous. Very large interior forces become percussion stresses $\mathbf{\Sigma}$ and percussions $\mathbf{R}$. The percussions and percussion stresses can be thought of as time concentrated quantities which define an atomic measure (a Dirac measure) and intervene only at collision times. The different virtual works are linear functions of the virtual velocities. They involve the percussions and percussion stresses.

The interior virtual work we choose is a linear function of the virtual strain rate and reads

$$\mathcal{T}_{\rm int}\left(\mathbf{v}\right) = -\int_{\Omega\setminus\Gamma} \mathbf{\Sigma} : \mathbf{E}\left(\frac{\mathbf{v}^+ + \mathbf{v}^-}{2}\right) d\Omega \qquad (1)$$

$$-\int_{\partial\Omega_1} \mathbf{R}\cdot\left(\frac{\mathbf{v}^+ + \mathbf{v}^-}{2}\right) d\Gamma + \int_{\Gamma} \mathbf{R}\cdot\left\{\frac{\mathbf{v}^+ + \mathbf{v}^-}{2}\right\} d\Gamma\,,$$

where $\mathbf{E}(\mathbf{v}) = \nabla_{sym}\mathbf{v}$ is the classical symmetric strain rate tensor, $\mathbf{v}^+$ and $\mathbf{v}^-$ are virtual velocity fields. The fracture Γ is oriented thus we are allowed to consider a "left" part ($\mathbf{v}_l$) and a "right" part ($\mathbf{v}_r$) of the velocity field. So, the spatial velocity discontinuity is denoted $\{\mathbf{v}\} = \mathbf{v}_r - \mathbf{v}_l$.

The densities with respect to the Dirac measure are percussion stress tensors and interaction percussions between the solid and the obstacle as well as percussions between fracture surfaces. Percussions are generalized interior forces which appear when collisions occur. They are, as said earlier, usual interior forces concentrated in a very short period of time.

ISBN 978-3-901608-32-2

The virtual work of the acceleration forces is

$$\mathcal{T}_{\text{acc}}(\mathbf{v}) = \int_{\Omega} \rho[\mathbf{u}] \cdot \left(\frac{\mathbf{v}^+ + \mathbf{v}^-}{2}\right) d\Omega\,, \qquad (2)$$

where ρ is the solid density and $[\mathbf{u}] = \mathbf{u}^+ - \mathbf{u}^-$ is the velocity discontinuity in the collision and $\rho[\mathbf{u}]$ is the collision inertial percussion. We may note that the actual work of the acceleration forces is equal to the variation of the kinetic energy during collision. Moreover, for the sake of completeness, we assume an external percussion $\mathbf{R}_{ext}$ concomitant to the collision may be applied on boundary portion $\partial\Omega_2 = \partial\Omega/\partial\Omega_1$

$$\mathcal{T}_{\text{ext}}(\mathbf{v}) = \int_{\partial\Omega_2} \mathbf{R}_{ext} \cdot \left(\frac{\mathbf{v}^+ + \mathbf{v}^-}{2}\right) d\Omega\,. \qquad (3)$$

This problem has been analyzed in [6]. A variational problem is proposed and its solution is studied in the space of special functions with bounded deformation. Besides, in [7] a 1-D example is proposed.

2.1 Regularized approach

Numerical solution of the previous problem presents a major difficulty due to the unknown positions of fracture surfaces Γ (free discontinuities). So, we propose a regularized approach in the context of fracture damage mechanics. In particular, we introduce a spatial damage variable $\beta \in [0,1]$ that approximately describes the zone where the material is fractured. In fact, $\beta = 1$ represents the sound material while $\beta = 0$ is equivalent to the completed damaged state. The main idea, firstly proposed in [8] and [9], is based on adaptation of the principle of virtual work. In particular, we assume that damage results from microscopic motions, and include the work of these motions in the principle of virtual work. This contribution is assumed to depend on the rate of damage and on the rate of the damage gradient. The damage gradient is introduced to account for the local interaction of the damage at a material point on the damage of its neighborhood. So, the internal virtual work (1) is replace by

$$\begin{aligned}\mathcal{T}_{\text{int}}(\mathbf{v}, b) = &-\int_{\Omega} \boldsymbol{\Sigma} : \mathbf{E}\left(\frac{\mathbf{v}^+ + \mathbf{v}^-}{2}\right) d\Omega \\ &-\int_{\partial\Omega_1} \mathbf{R} \cdot \left(\frac{\mathbf{v}^+ + \mathbf{v}^-}{2}\right) d\Gamma \\ &-\int_{\Omega} \{B[b] + \mathbf{H} \cdot grad[b]\} d\Omega\,, \end{aligned} \qquad (4)$$

where $\mathbf{v}^+$, $\mathbf{v}^-$ and b^+, b^- are virtual velocities. The first and the second terms are classical and are related to the mechanical action and reactions. The third and fourth terms are new: B is a mechanical work, in particular the internal damage work which is responsible for the evolution of the damage during the collision. $\mathbf{H}$ is a flux vector responsible for the interaction of the damage at a point on the damage on its neighborhood.

3 The equations of motion

The principle of virtual work

$$\forall\, \mathbf{v}, b \quad \mathcal{T}_{\text{acc}}(\mathbf{v}) = \mathcal{T}_{\text{int}}(\mathbf{v}, b) + \mathcal{T}_{\text{ext}}(\mathbf{v})\,, \qquad (5)$$

gives two sets of equations of motion. By choosing convenient virtual velocity, we obtain

$$\rho[\mathbf{u}] = div\boldsymbol{\Sigma}\,, \quad \text{in } \Omega\,, \qquad (6)$$

$$\boldsymbol{\Sigma} \cdot \mathbf{n} = -\mathbf{R} \quad \text{on } \partial\Omega_1\,, \qquad (7)$$

$$\boldsymbol{\Sigma} \cdot \mathbf{n} = \mathbf{R}_{ext} \quad \text{on } \partial\Omega_2\,, \qquad (8)$$

$$div\mathbf{H} - B = 0 \quad \text{in } \Omega\,, \qquad (9)$$

$$\mathbf{H} \cdot \mathbf{n} = \mathbf{0} \quad \text{on } \partial\Omega\,, \qquad (10)$$

where $\mathbf{n}$ is the outward normal to Ω. Equations (6)-(10) are the equations of motion accounting for macroscopic and microscopic effects.

4 The constitutive laws

For the sake of simplicity we assume the temperature to be constant though the thermal effects are important and may be taken into account, [4]. In our problem we assume that the velocity $\mathbf{u}^-$, supposed for the sake of simplicity to be a rigid body velocity, and the damage β^- before the collision are assigned and let the unknowns be the velocity $\mathbf{u}^+$ and the damage β^+ after the collision. The constitutive laws, which have to satisfy the second law, for the mechanical and damage interior forces are defined by three functions: the volume free energy Ψ, the volume dissipative function Φ and the contact surface with the obstacle pseudo-potential of dissipation Φ_s. We have to choose them in such a way that β^+ is zero in thin layers and 1 elsewhere and in such a way the strain rate is very large in the thin layer and almost zero else where. We choose the volume free energy as

$$\begin{aligned}\Psi(\varepsilon, \beta, grad\beta) = w(1-\beta) \\ +\frac{k}{2}(grad\beta)^2 + \frac{\beta}{2}\varepsilon\mathbf{C}\varepsilon + I(\beta)\,. \end{aligned} \qquad (11)$$

The volume dissipative function is addressed as follows

$$\begin{aligned}\Phi\left(\mathbf{E}\left(\frac{\mathbf{u}^+ + \mathbf{u}^-}{2}\right), [\beta], grad[\beta]\right) = \frac{c}{2}[\beta]^2 \\ +\frac{\mu}{q}\left(\beta^- + \frac{[\beta]}{2}\right)\left\|\mathbf{E}\left(\frac{\mathbf{u}^+ + \mathbf{u}^-}{2}\right)\right\|^q + \\ +\frac{\lambda}{r}\left\|\mathbf{E}\left(\frac{\mathbf{u}^+ + \mathbf{u}^-}{2}\right)\right\|^r \\ +I_-([\beta]) + I_+\left(div\left(\frac{\mathbf{u}^+ + \mathbf{u}^-}{2}\right)\right)\,. \end{aligned} \qquad (12)$$

The contact surface with the obstacle pseudo-potential of dissipation is

$$\Phi_s\left(\frac{\mathbf{u}^+ + \mathbf{u}^-}{2}\right) = \lambda_s\left(\frac{\mathbf{u}^+ + \mathbf{u}^-}{2}\right)^2 + I_-\left(u_n^+\right)\,. \qquad (13)$$

The quantity w is the cohesion of the material, $\mathbf{C}$ is the classical elasticity tensor, ε the deformation tensor which does not change during collision and k is the damage collision coefficient which quantifies the influence of the damage at a point onto the damage of its neighborhood. The parameters c, λ, μ, λ_s characterize the microscopic and macroscopic dissipations. The exponents $r \in]0,1[$ and $q \in]1,2]$ indicate the nature of the behaviour of the constitutive law: convex or concave. In particular, the convex term involving the strain rate $\mathbf{E}$ consists of the visco-plastic Norton-Hoff-Friaa potential which approximates the perfect plastic potential, when q tends to one. Moreover, the effect of the concave term with power r lower than 1 is to avoid having many regions with small discontinuities and to have the strain rates very large in thin damaged zones.

The functions I, I_-, I_+ are the indicator functions of the intervals $[0,1]$, ($I(\gamma)=0$, if $0 \le \gamma \le 1$ and $I(\gamma) = +\infty$, if $\gamma \notin [0,1]$), of $]-\infty, 0] = \mathbb{R}^-$, ($I_-(\gamma) = 0$, if $\gamma \le 0$ and $I_-(\gamma) = +\infty$, if $\gamma > 0$), and of $[0, \infty[= \mathbb{R}^+$, ($I_+(\gamma) = 0$, if $\gamma > 0$ and $I_+(\gamma) = +\infty$, if $\gamma < 0$), (see [10]). The indicator functions take care of the internal constraints

$$\beta \in [0,1]\,,\ [\beta] \le 0,\ u_n^+ \le 0,\ div\left(\frac{\mathbf{u}^+ + \mathbf{u}^-}{2}\right) \ge 0\,. \tag{14}$$

The first internal constraint results from the definition of damage. The second constraint means that the solid does not mend during the collision. The other constraints are related to the velocity field and take into account impenetrability conditions: the first is on the obstacle contact surface and the last one, following an idea of Jean Jacques Moreau [11], replaces the impenetrability condition on the fractures by a volume non overlapping condition.

The norm of symmetric tensor $\mathbf{A}$ is defined as

$$\|\mathbf{A}\| = \sqrt{A_{ij}A_{ij}} = \sqrt{\mathbf{A}^2}\,. \tag{15}$$

The previous functions give the following set of constitutive laws

$$\begin{aligned}\mathbf{\Sigma} = \lambda \left\|\mathbf{E}\left(\frac{\mathbf{u}^+ + \mathbf{u}^-}{2}\right)\right\|^{r-2} \mathbf{E}\left(\frac{\mathbf{u}^+ + \mathbf{u}^-}{2}\right) \qquad (16)\\ +\mu\left(\frac{\beta^- + \beta^+}{2}\right)\left\|\mathbf{E}\left(\frac{\mathbf{u}^+ + \mathbf{u}^-}{2}\right)\right\|^{q-2} \mathbf{E}\left(\frac{\mathbf{u}^+ + \mathbf{u}^-}{2}\right) \\ -p\mathbf{I}\,,\end{aligned}$$

$$\begin{aligned}B \in -w + \frac{1}{2}\varepsilon\mathbf{C}\varepsilon + \partial I\left(\beta^+\right) + c\,[\beta] \qquad (17)\\ +\frac{\mu}{2q}\left\|\mathbf{E}\left(\frac{\mathbf{u}^+ + \mathbf{u}^-}{2}\right)\right\|^q + \partial I_-\left([\beta]\right)\,,\end{aligned}$$

$$\mathbf{H} = k\,grad\beta^+\,, \tag{18}$$

$$\mathbf{R} \in \lambda_s(\mathbf{u}^+ + \mathbf{u}^-) + \partial I_-\left(u_n^+\right)\mathbf{n}\,, \tag{19}$$

where

$$-p \in \partial I_+\left(\frac{\mathbf{u}^+ + \mathbf{u}^-}{2}\right)\,. \tag{20}$$

The subdifferential sets ∂I_+ and ∂I_- of the indicator functions of the positive and negative numbers R^+ R^- are defined as: $\partial I_+(0) = R^-$, $\partial I + -(\gamma) = 0$ for $\gamma > 0$ and $\partial I_+(\gamma) = \emptyset$ for $\gamma < 0$, $\partial I_-(0) = R^+$, $\partial I_-(\gamma) = 0$ for $\gamma < 0$ and $\partial I_-(\gamma) = \emptyset$ for $\gamma > 0$. The quantity $\partial I_-\left(u_n^+\right)\mathbf{n}$ is the impenetrability percussion reaction. It is active only if the other interactions are not sufficient for the solid and the plane not to interpenetrate, i.e., when the normal velocity after the collision is 0. The quantity $-p$ is the internal impenetrability pressure. This reaction prevents the volume overlapping. From the numerical simulations proposed in section 6 clearly outcomes that $-p$ is active only in the fractured zones in compression or in the fragmented regions, avoiding interpenetration. In fact, the undamaged portions of the solid after collision have nearly rigid body velocity.

Let us note that the second law of thermodynamics equivalent to the following inequality is satisfied for $r \in]0,1[$ and $q \in]1,2]$, [4]

$$\begin{aligned}\mathbf{\Sigma} : \mathbf{E}\left(\frac{\mathbf{u}^+ + \mathbf{u}^-}{2}\right) + B\,[\beta] - [\Psi] \ge \qquad (21)\\ \mu\left(\frac{\beta^- + \beta^+}{2}\right)\left\|\mathbf{E}\left(\frac{\mathbf{u}^+ + \mathbf{u}^-}{2}\right)\right\|^q \\ +\lambda\left\|\mathbf{E}\left(\frac{\mathbf{u}^+ + \mathbf{u}^-}{2}\right)\right\|^r - w\,[\beta] + c\,[\beta]^2 \\ +\frac{\mu}{2q}\,[\beta]\left\|\mathbf{E}\left(\frac{\mathbf{u}^+ + \mathbf{u}^-}{2}\right)\right\|^q + \partial I_-\left([\beta]\right)[\beta] \\ +\partial I\left(\beta^+\right)[\beta] + k\,grad\beta^+\,grad\,[\beta] \ge 0\,.\end{aligned}$$

5 The equations

The principle of virtual work and a proper use of the constitutive laws leads to two sets of equations and permits to compute the velocity and damage of the body after the collision depending on the incoming velocity and the damage state before the collision.

For simplicity, we assume the body is undamaged before the collision, that its velocity is a rigid body velocity and that it is not deformed before collision

$$\beta^- = 1, \quad \mathbf{E}(\mathbf{u}^-) = 0, \quad \varepsilon = 0\,. \tag{22}$$

Moreover, assuming (22) it results

$$\partial I(\beta^+) + \partial I_-(\beta^+ - 1) = \partial I(\beta^+)\,. \tag{23}$$

So, the equations to find $\mathbf{u}^+$ and β^+ are

$$\rho\mathbf{u}^+ - div\mathbf{\Sigma}(\mathbf{u}^+) = \rho\mathbf{u}^-\,, \quad \text{in } \Omega\,, \tag{24}$$

$$\mathbf{\Sigma}\cdot\mathbf{n} + \lambda_s(\mathbf{u}^+ + \mathbf{u}^-) + \partial I_+(u_n^+)\mathbf{n} \ni 0 \quad \text{on } \partial\Omega_1\,, \tag{25}$$

$$\mathbf{\Sigma}\cdot\mathbf{n} = \mathbf{R}_{ext} \quad \text{on } \partial\Omega_2\,, \tag{26}$$

$$\begin{aligned}c\beta^+ - k\triangle\beta^+ + \partial I(\beta^+) \ni \qquad (27)\\ w + c - \frac{\mu}{2q}\left\|\mathbf{E}\left(\frac{\mathbf{u}^+}{2}\right)\right\|^q \quad \text{in } \Omega\,,\end{aligned}$$

$$\frac{\partial \beta^+}{\partial \mathbf{n}} = 0 \quad \text{on } \partial\Omega\,. \tag{28}$$

6 Numerical examples

In this section three numerical experiments are presented. Let us emphasize that we do not try to compare our results with those of actual experiments - this will be object of a forthcoming investigation - but to illustrate the capability of the proposed model to describe different failure modes. In particular, after collision the material may present three different states: not fractured, fractured, fragmented. In details, the not fractured region is represented by the undamaged zone ($\beta(x) = 1$), the fractured state presents completed damaged materials with an opening mode (i.e., $\mathrm{div}(\mathbf{u}^+) > 0$) or in compression regime (i.e., $\mathrm{div}(\mathbf{u}^+) = 0$) while the fragmented regions are diffused damaged zones mainly due to very high strain rate gradients.

Moreover, we restrict our attention to the case of a 2-dimensional problems in plane strain condition of a single deformable body colliding a rigid, immobile obstacle.

The discrete solutions, obtained via finite element method, involves the resolution of a non-linear non convex minimization problem. The solution is obtained by an iterative calculation with a sequence of decreasing parameter $q \to 1$ starting from a quadratic convex term ($q = 2$). Specially, the calculation can be stopped at any iterative step and restart from the previous solution even with an updated parameter q. This technique demonstrates to considerably speed up numerical convergence. Kinematical constraints are introduced by duality via the well known technique of the Lagrange multipliers. An ad-hoc Uzawa algorithm has been developed for the resolution of the resulting saddle point problem.

6.1 Falling Bar

We consider the case of a slender rectangular bar colliding three rigid supports. Prior the collision, the bar is assumed to be undamaged ($\beta^-(x) = 1$) and falls with a constant vertical descending velocity (see Fig. 1). The predictive theory gives the velocity and damage after collision, $\mathbf{u}^+(x)$ and $\beta^+(x)$, depending on falling velocity $\mathbf{u}^-$. Two representative cases have been analyzed: all the parameters are fixed except the density of the material thus an heavy material and a light material, having the same resistance, have been considered (a ratio between the material densities equal to 10 has been adopted).

In Figure 2 is represented the damage field $\beta(x)$ for different incoming velocities for the case of the heavy material. From Figure 2 clearly outcomes that the failure process can be classified with three states depending on the amount of imparted energy $\sim (\mathbf{u}^-)^2$: not fractured, fractured and fragmented states with a rather sharp transition in between. For value of u^- smaller than $1\,m/s$, no fracture appears in the solid. For $1.5625 \le u^- \le 3.125\,m/s$ well defined fractures appears in the solids. It may be noted that the fractured portions of solid in

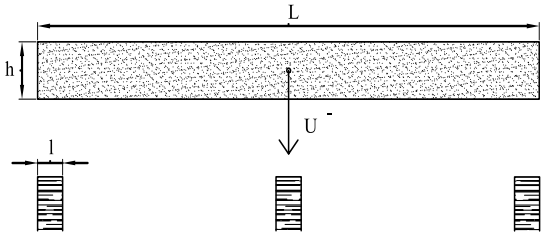

Fig. 1 Bar falling onto three rigid supports. The length of the bar is $L = 4$ m and ratio $L/l = 20$ and $h/l = 0.8$ have been assumed. The other parameters have the following value: $\mu = 5.e2$, $\lambda = 1.e2$, $\rho = 3.e3$ or $3.e2$, $p = 0.5$, $q = 1.01$, $c = 3.e3$, $k = 0.1$, $w = 1.e2$, $\lambda_s = 2.e3$.

compression are larger than those in traction. Intermediate incoming velocity value $6.25 \le u^- \le 12.5\,m/s$ outlines the coexistence of the fractured and fragmented states. In fact, if above the rigid supports fragmented regions appear after collision, well defined fractures are still present inside the solid. Differently, high values of the impact velocity do not allowed the creation of well defined fractures and only fragmentation due to the large percussion transmitted between the solid and the rigid obstacles is present. It is important to note that the fragmented parts of the solids do not change a lot passing from $u^- = 25\,m/s$ to $u^- = 50\,m/s$ even if the kinetic energy becomes four times higher.

In Figure 3 the velocity field $\mathbf{u}^+(x)$ is reported for the case $u^- = 1.5625\,m/s$. The bar is broken into five pieces after the collision. A central block stops above the central obstacle while instantaneous rigid rotations in the other block are induced by fracture creations.

This fact is shown by the representation of the horizontal displacement along two straight horizontal lines located at different positions reported in Figure 4. Strong discontinuities in the displacement behaviour are localized in the fractured regions while the remaining pieces of the solid undergo a nearly rigid body motions. Moreover, the fractures in opening mode are outlined by the representation of the divergence of the velocity field reported in Figure 5.

Similar considerations maybe done for the case of $u^- = 3.125\,m/s$ reported in Figures 6 and 7 except by the fact that the bar breaks into seven pieces.

In Figure 8 is represented the damage field $\beta(x)$ for different incoming velocities for the case of the light material. In Figures 9-12 are reported the velocity fields and $div(\mathbf{u}^+)$ for two different values of falling velocity: $u = 6.25, 12.5\,m/s$. The main differences with respect to the previous case can be summarized as follow:

- because of minor weight of the body, rebounds occur on the obstacles. This a general property of collisions both theoretical and experimental, [4];
- the central crack is completely different in this case: it is induced by rebound of the central portion;

- for high velocity values the light body breaks in several parts while the heavy material is cut into two elements.

6.2 Annular disk

The proposed model has been applied to the case of an annular disk falling with a rigid vertical velocity and colliding with a fixed rigid floor. In Figures 13-16 are represented the damage field, the divergence of the velocity field $\mathbf{u}^+$ after the collision and the horizontal and the vertical components of the velocity field. We only underline the fact that two failure zones appear in the ring after collision. A first major fragmented zone is above the contact surface and involves the entire thickness of the annulus while in the opposite part a well defined fracture is produced along the vertical direction.

6.3 Impact simulation

As a third example we reproduced qualitatively the impact tests reported in [12]. They illustrated different impact tests on reinforced concrete slabs with the machine reported in Figure 17. The aim of this example is to show the capability of the proposed model to simulate actual experiments and we do not want to compare numerical results with experimental evidences. First of all, we consider a simplified 2D example. Left and right extremities are clamped while a percussion is applied on the impact surface. Moreover we do not take into account the metallic reinforcements. In Figures 18-21 are represented the damage field, the divergence of the velocity field $\mathbf{u}^+$ after the collision and the horizontal and the vertical components of the velocity field. Different failures are outlined from these Figures.

7 Conclusions

In this predictive theory for collisions and fractures only macroscopic quantities are involved. The equations of motion are derived from the principle of virtual work where new interior forces are introduce to describe the very large stresses and the very large contact forces resulting from the cinematic incompatibilities. The theory of collisions and fracture of solids outlined in this article is consistent from the mechanical point of view and it has good mathematical formulations to which adapted numerical methods may be applied.

Some numerical simulations have been performed via the classical finite element method, concerning a solid colliding against a rigid fixed obstacle or a clamped solid subjected to high velocity impact. Numerical results shown a strong versatility of the model to describe different failure modes. Let us also stress that few parameters are involved, less than 9, to predict at the engineering level solid fracturation.

8 References

[1] W. L. Fourney. Mechanisms of rock fragmentations by blasting. volume 4, pages 39–69. Pergamon, Oxford, 1993.

[2] H. Romero. *Fragmentation du béton sous explosion*. PhD thesis, Université de Montpellier II, Montpellier, France, 2003.

[3] M. Frémond. *Non-smooth thermomechanics*. Springer Verlag, Heidelberg, 2001.

[4] M. Frémond. *Collisions*. Edizioni del Dipartimento di Ingegneria Civile dell'Università di Roma Tor Vergata, Rome, 2007.

[5] M. Frémond, R. Gormaz, and J. A. Martín. Collision of a solid with an incompressible fluid. *Theoretical and Computational Fluid Dynamics*, 16:405–420, 2003.

[6] E. Bonetti and M. Frémond. Collisions and fractures: a model in SBD. *Rend. Mat. Acc. Lincei*, 15(9):47–57, 2004.

[7] E. Bonetti and M. Frémond. Collisions and fractures: a 1-D theory. how to tear off a chandelier from the ceiling. *J. of Elasticity*, 15(9):47–57, 2004.

[8] M. Frémond. Adhérence des solides. *J. de Mécanique théorique et appliquée*, 6:383–407, 1987.

[9] M. Frémond and B. Nedjar. Damage, gradient of damage and principle of virtual power. *Int. J. Solids Structures*, 8:1083–1103, 1996.

[10] J. J. Moreau. Fonctionelles convexes - Séminaire sur les équations aux dérivées partielles. Edizioni del Dipartimento di Ingegneria Civile dell'Università di Roma Tor Vergata, Roma - Collége de France, Paris, 2003 - 1966.

[11] J. J. Moreau. Principes extrêmaux pour le problème de la naissance de la cavitation. *Journal de Mécanique*, 5:439–470, 1966.

[12] M. Zineddin and T. Krauthammer. Dynamic response and behavior of reinforced concrete slabs under impact loading. *Int. J. of Impact Engineering*, 34:1517–1534, 2007.

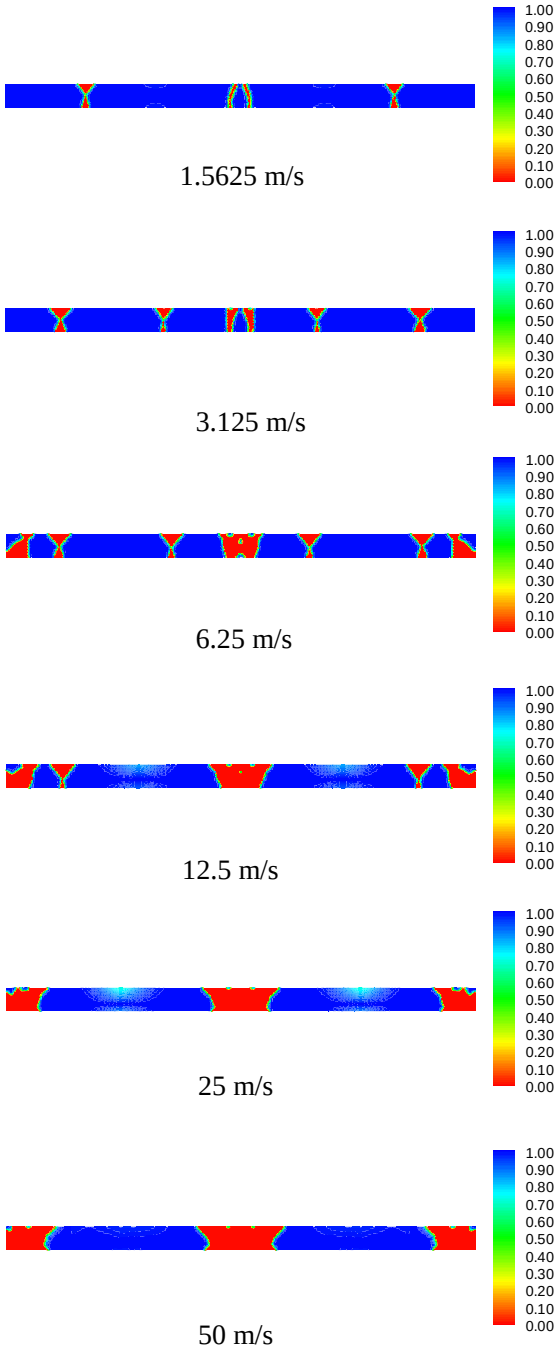

Fig. 2 Damage in a heavy bar falling at different velocities. The blue zone is not damaged. The thin red zones are damaged. They account for fractures. When the falling velocity is very large, the damaged zones become completely fragmented domains

Fig. 3 Velocity $\mathbf{u}^+(x)$ after the collision for $u^- = 1.5625\,m/s$. The bar is broken into five pieces. The pieces do not bounce on the obstacles

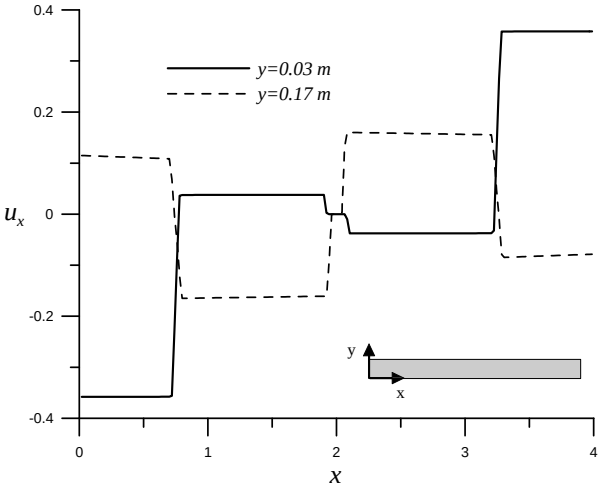

Fig. 4 Horizontal displacement along two straight horizontal lines located at different positions for $u^- = 1.5625\,m/s$. The vertical distances y are measured from the bottom of the beam. The strong discontinuities in the displacement values outlined the fractures while the remaining pieces of the solids undergo a nearly rigid body motions. Note the 0 velocity of the central piece on the central obstacle.

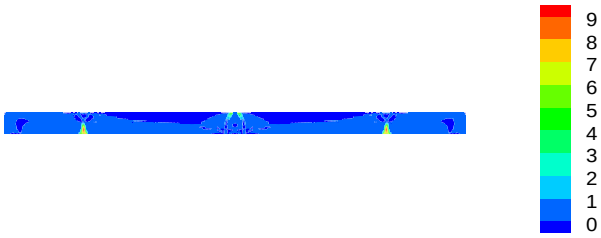

Fig. 5 The divergence of the velocity vector after the collision for $u^- = 1.5625\,m/s$. The opening fractures are represented by zone with high values of $\mathrm{div}(\mathbf{u}^+(x))$.

Fig. 6 Velocity $\mathbf{u}^+(x)$ after the collision for $u^- = 3.125\,m/s$. The bar is broken into seven pieces.

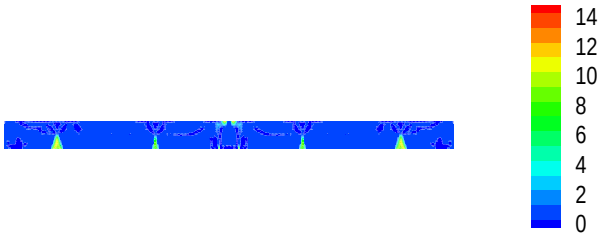

Fig. 7 The divergence of the velocity vector after the collision for $u^- = 3.125\,m/s$. The opening fractures are represented by zone with high values of $\mathrm{div}(\mathbf{u}^+(x))$.

ISBN 978-3-901608-32-2

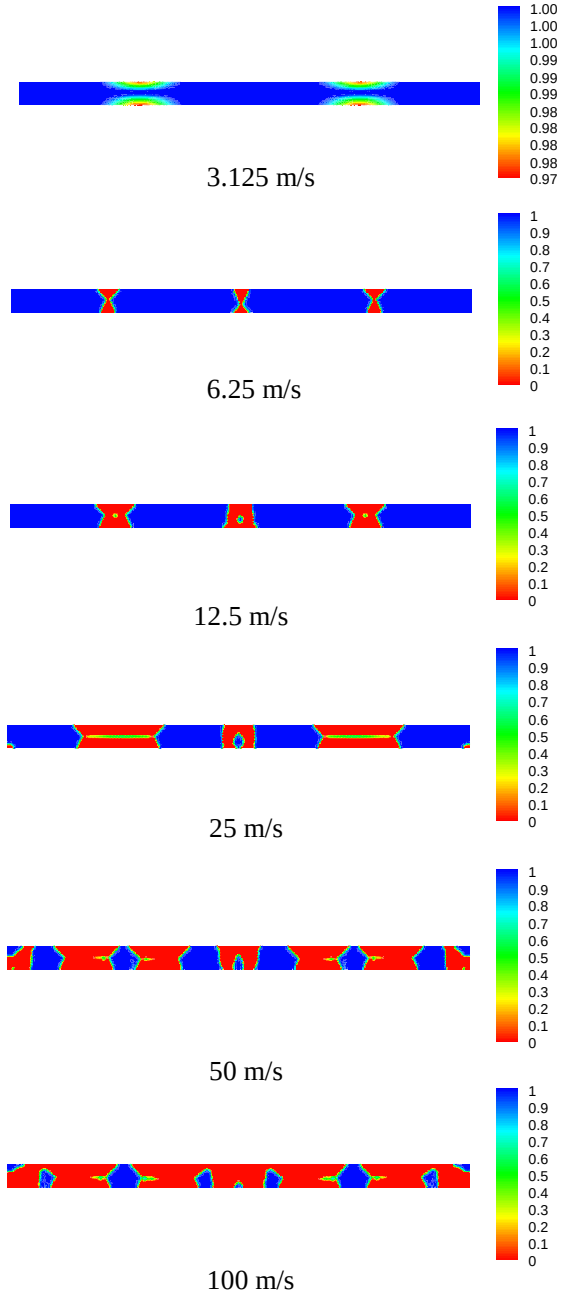

Fig. 8 Damage in a light bar falling at different velocities. The blue zone is not damaged. The thin red zones are damaged. They account for fractures. When the falling velocity is very large, the damaged zones become completely fragmented domains

Fig. 9 Velocity $\mathbf{u}^+(x)$ after the collision for $u^- = 6.25\,m/s$. The bar is broken into four pieces which bounce on the obstacles

Fig. 10 The divergence of the velocity vector after the collision for $u^- = 6.25\,m/s$. The opening fractures are represented by zone with high values of div$(\mathbf{u}^+(x))$.

Fig. 11 Velocity $\mathbf{u}^+(x)$ after the collision for $u^- = 12.5\,m/s$. The bar is broken into four pieces which bounce on the obstacles.

Fig. 12 The divergence of the velocity vector after the collision for $u^- = 12.5\,m/s$. The fractures are represented by zone with high values of div$(\mathbf{u}^+(x))$.

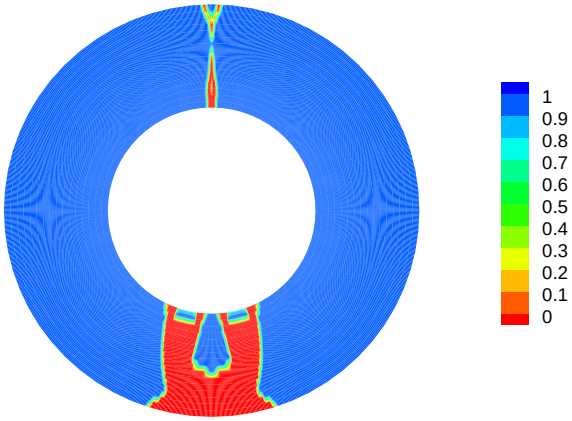

Fig. 13 Damage field β^+ after collision.

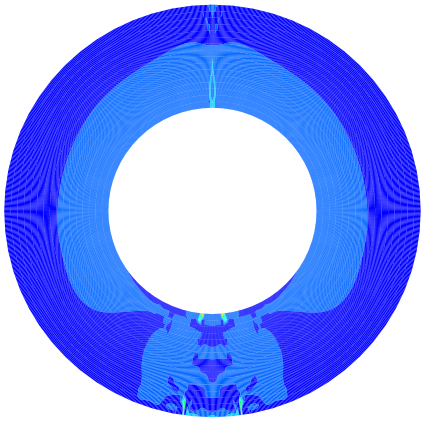

Fig. 14 Divergence of the velocity field after collision $\mathrm{div}(\mathbf{u}^+(x))$.

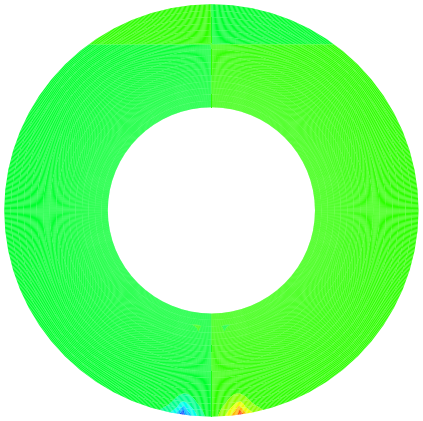

Fig. 15 Horizontal component u_x of the velocity field.

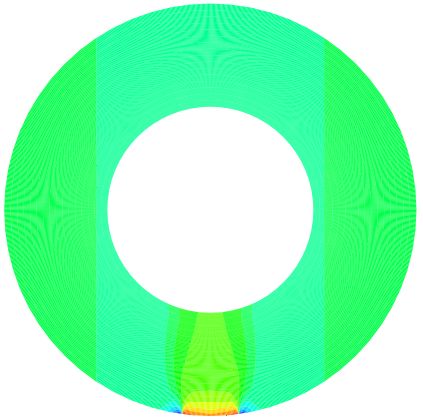

Fig. 16 Vertical component u_y of the velocity field.

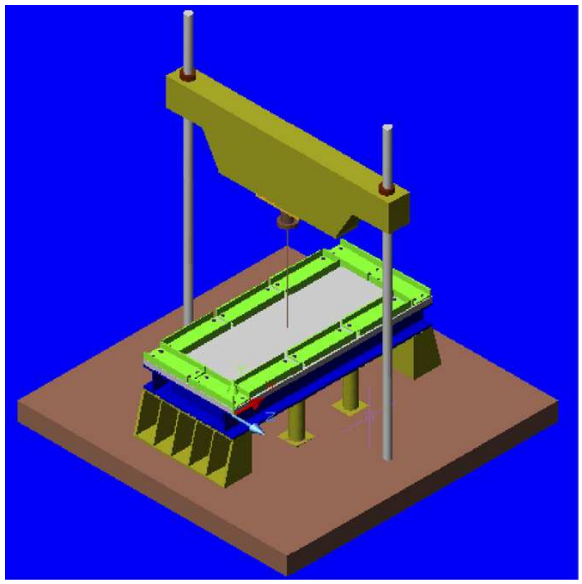

Fig. 17 Precision impact testing system proposed in [12].

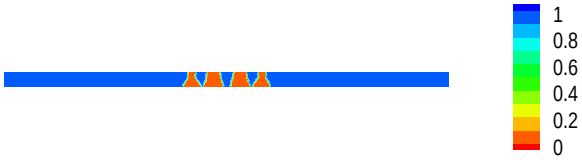

Fig. 18 Damage field after impact.

Fig. 19 Velocity field after impact.

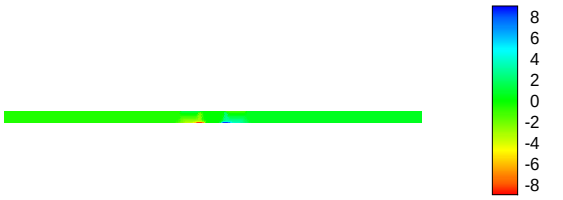

Fig. 20 Horizontal component u_x of the velocity field.

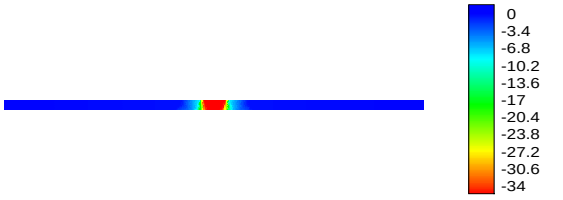

Fig. 21 Vertical component u_y of the velocity field.

